VISUALIZATION OF OXYGEN CONCENTRATION FIELDS IN THE WAKE OF BUBBLES BY PLANAR LASER INDUCED FLUORESCENCE

M. JIMENEZ[1,2,3,c], M. LE BIGAUT[1,2,3], N. DIETRICH[1,2,3], G. HEBRARD[1,2,3]

[1]Université de Toulouse, INSA,UPS,INP, LISBP, 135 Avenue de Rangueil, F-31077 Toulouse, France
[2]INRA, UMR792, Ingénierie des Systèmes Biologiques et des Procédés, F-31400 Toulouse, France
[3] CNRS, UMR5504, F-31400 Toulouse, France
[c] Corresponding author: Tel.: +561559798; Email: mjimenez@insa-toulouse.fr

KEYWORDS:
Main subjects: mass transfer, bubble
Fluid: air, water
Visualization method(s): planar laser induced fluorescence (PLIF)

ABSTRACT

Visualization and quantification of mass transfer of air bubbles in different liquid media, using the Planar Laser-Induced Fluorescence (PLIF) technique, is studied in this paper. This technique is based on the introduction of a fluorescent dye in the liquid phase whose light emission level depends on the oxygen concentration in the medium. Oxygen concentration profiles are then obtained in the wake of the rising studied bubble, along a horizontal direction. These profiles are then used to determine both the oxygen flux transferred by the bubble and the liquid side mass transfer coefficient k_L. The considered technique has been applied to bubbles of different scales, including also non spherical bubbles ($0.7<d_{bubble}<3$ mm) and results have been compared with values of literature.

INTRODUCTION

Study of mass transfer at a gas-liquid interface is of prime interest in different domains of study such as wastewater treatment, chemical processes, and environmental issues (transfer of pollutants, *etc*.). In many industrial applications, this transfer often happens at a bubble-liquid interface to enhance mass transfer and improve the corresponding process efficiency. As an example, such a process is involved in aeration tank in wastewater treatment. In these conditions, a global characterization of the transfer is usually achieved, based for instance on probe measurements. These techniques often allow the volumetric mass transfer coefficient $k_L \times a$ to be determined, where k_L (m/s) is the liquid side mass transfer coefficient and a the interfacial aera (m^2/m^3). However, it has been shown that the two factors (k_L and a) can evolved differently depending on the varying parameters[1] while determining separately k_L and a can be difficult. As a consequence, this global approach can be inefficient to understand physical phenomena at such interfaces. To alleviate this problem, some studies adopted a local approach and PLIF is a powerful laser technique for that purpose. PLIF is based on the introduction of a fluorescent dye in the liquid phase, which is able to re-emit light when exited by an appropriate light (generally coming from a laser source). The fluorescent dye can be chosen depending on its sensitivity to some parameters (such as oxygen concentration, pH, temperature changes, *etc*.). In our case, when oxygen transfers in the liquid phase and due to the collision between molecules, oxygen is able to absorb the excess energy of the dye. The dye can thus return to its fundamental state by a non radiative process[2]. As a consequence, the oxygen concentration is highly related to the recorded fluorescence level. This technique has been mainly used to visualize the gas transfer in the wake of rising bubbles[3,4,5]. However, the experimental set-ups proposed for visualization were not well adapted for quantification mainly due to the reflexion and the drop shadow that appear at the bubble neighborhood (Figure 1). To avoid this problem, a new experimental set-up has been proposed by Francois *et al.* (2011)[6]. Contrary to the previous studies based on a lateral view of the transfer phenomenom (*cf.* Figure 1), the transfer is observed along a horizontal section in the wake of the bubble.

Using this visualization along the horizontal section allows the field of oxygen transfer to be visualized and quantified. A mathematical analysis that will be briefly commented in this paper has been proposed to determine both the flux of oxygen and the liquid side mass transfer coefficient k_L. The purpose of this paper is to verify if the previous work of Francois *et al.* (2011) can be extended to the case of non-spherical bubbles.

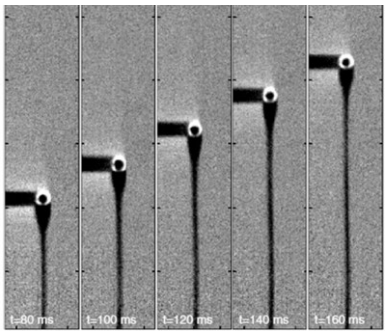

Figure 1. Lateral view of CO2 transfer in the wake of a bubbles based on Stöhr (2009)[3]

EXPERIMENTAL SET-UP

As explained above, the experimental set-up (Figure 2) has been designed to visualize oxygen transfer (4) according to a horizontal section in the wake of the bubble (5).

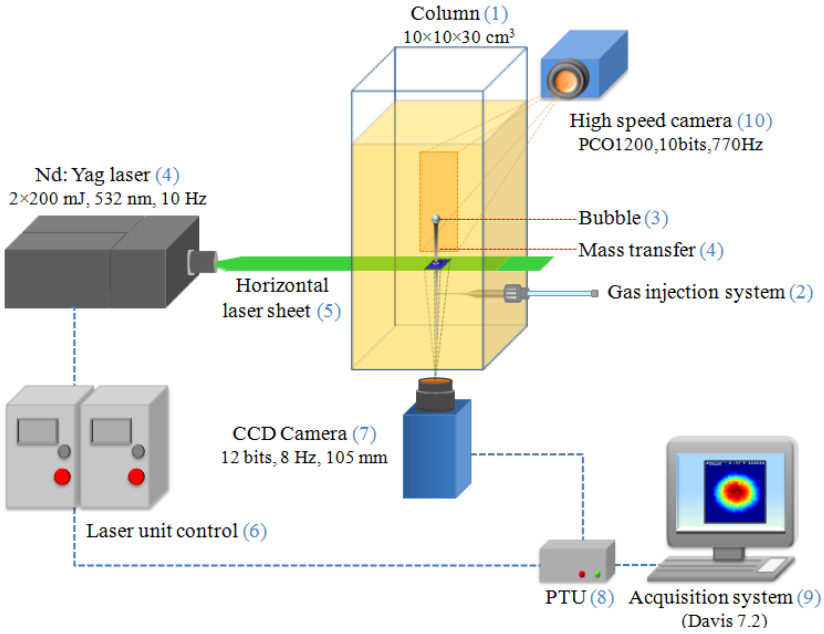

Figure 2. Experimental set-up

An air bubble is injected (2) into the transparent column (1) (10×10×30 cm^3) filled with the liquid of interest previously deoxygenated using nitrogen. To observe the fluorescence phenomenom, 25 mg/L of Ruthenium complex ($C_{72}H_{48}N_8O_6Ru$, Nanomeps) has been added to the liquid. The main advantage of this fluorescent dye is its sensitivity to the presence of oxygen. However, since it is not water-soluble, 20% w/w of ethanol has also been added to the media. To excite the fluorescent dye, a laser sheet (5), is horizontally generated by a Nd: Yag laser (4) (Quantel, λ = 532 nm, 10 Hz, 2×200 mJ) about 10 cm above the column bottom. The fluorescence level in the wake of the bubble is recorded by a CCD camera (7) (Imager Intense, LaVision, Germany, 12 bits, 1040×1376 $pixels^2$) located under the column A 105 mm objective (Micro-Nikkor 105 mm f/8, Nikon) and three teleconverters were added to the digital camera to obtain a focused area of about 3×4 mm^2. Since the Ruthenium complex emits around 670 nm, a 570 nm high-pass filter was also placed on the camera to register its fluorescence and to block the laser light. A high speed camera (PCO 1200, 10 bits,770 Hz,1024×1280 $pixels^2$) is placed orthogonally to the first one and above the laser sheet to record the velocity and the shape of the bubble (image area ≈ 3×4 cm^2). The laser and the CCD camera are synchronized by a Programmable Trigger Unit (LaVision).

The images recorded by the two cameras are visualized by specific acquisition softwares (Davis and CamWare). These images consist of fluorescence levels, characterized by grey levels whose values depend on the oxygen concentration. To estimate concentration profiles, the Stern-Volmer correlation is used.

$$\frac{I_Q}{I_0} = \frac{1}{1 + K_{SV}[Q]}$$

with I_Q and I_0 the fluorescence levels (characterized by grey levels) in presence and absence of quencher (O_2) respectively, K_{SV} the Stern-Volmer constant (L/mg), and $[Q]$ the concentration of the quencher (mg/L).
The fluorescence level of the solution is thus directly proportional to the inverse of the gas concentration in the liquid phase. Values of K_{SV} and I_0 have been determined using a calibration curve that corresponds to the fluorescence level measurement for different known and uniform oxygen concentrations in the liquid phase (ranging from about 0 mg/L to the saturation concentration of the gas, 9 mg/L) (Figure 3).

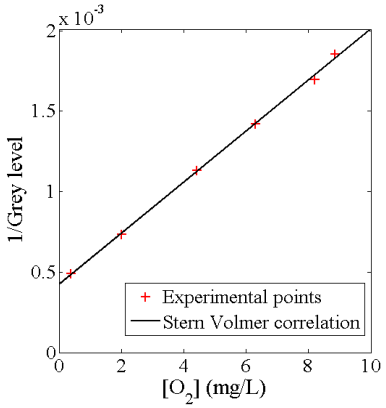

Figure 3. Calibration curve

This curve shows that fluorescence levels and oxygen concentrations are inversely proportional. Once the calibration step has been achieved, the quantification of mass transfer in the wake of the bubble is possible. Figure 4 illustrates the mass transfer phenomenon for different bubble size.

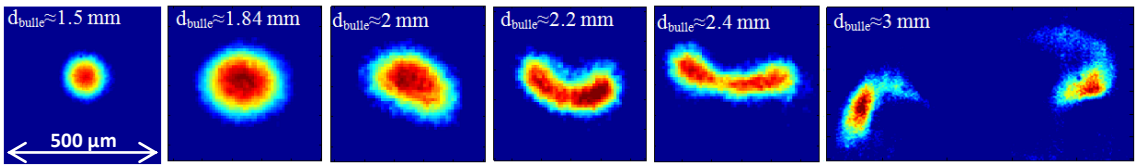

Figure 4. Visualization of oxygen mass transfer along a horizontal section for different bubble diameters.

It has already been observed that the transfer spots generated by small spherical bubbles, whose movement is vertical, are circular on the horizontal surface presented above. However, when considering the non-spherical case, the spot shape highly depends on the bubble shape. As an example, Table 1 shows the blinding coefficients of the bubbles depicted in Figure 4, defined as the ratio of the smallest and largest radius of the bubble as a function of the diameter of the bubble. This diameter has been defined as the equivalent diameter of a spherical bubble of same volume than the studied bubble. Velocities of these bubbles ranged from about 20 to up to 30 cm/s.

d_{bubble} of *Figure 4*	1.5 mm	1.84 mm	2 mm	2.2 mm	2.4 mm	3 mm
Blinding factor ε	1	0.7	0.55	0.53	0.51	0.48

Table 1. Blinding coefficients of the bubbles depicted in Figure 4.

For bubbles with diameter larger than 3 mm, the transfer dispersion in the wake of the bubble is too fast to be observed with the proposed experimental set-up. The next section presents a mathematical development to estimate the transferred flux and the mass transfer coefficient k_L for diameters smaller than 3 mm using images similar to those presented in Figure 4.

MATHEMATICAL RESOLUTION : SPHERICAL CASE

It is important to note that only the main steps of the method will be reported in this paper. The reader is invited to look at Francois *et al.* (2011)[6] for more details. The determination of the oxygen flux is obtained using a mass balance. Let consider a cylindrical parameterization and the following three domains (*cf.* Figure 5):

- ∂D_S, the upper cylinder surface, located above the bubble, where oxygen is still absent, leading to $[O_2] = 0$ mg/L.
- ∂D_B, the bubble surface, where liquid and bubble velocity are equal (by continuity of the velocity).
- ∂D_W, the lower cylinder surface, located below the bubble, where the liquid (initially of null velocity) is disrupted by the bubble and whose velocity is denoted as U_w.

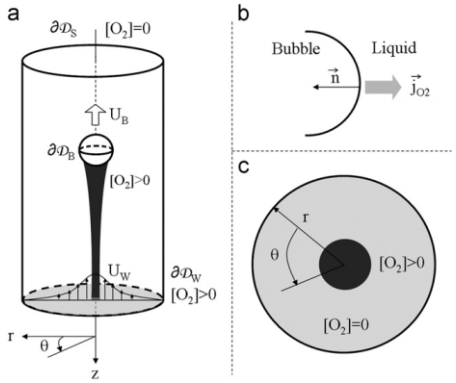

Figure 5. Domain definitions and notations for the mathematical resolution based on Francois et al.(2011)[6]

The oxygen accumulation in a domain ∂D can be decomposed as a sum of a convective and a diffusive term as follows

$$\frac{dm_{O2}}{dt} = -\oiint_{\partial D} (\vec{U} - \vec{U}_{\partial D})[O_2]\vec{n}dS - \oiint_{\partial D} \vec{j}_{O2}\vec{n}dS \qquad (1)$$

where m_{O2} is the mass of O_2 in mg, $\vec{U}$ (resp. $\vec{U}_{\partial D}$) is the liquid (resp. the surface) velocity in m/s, $[O_2]$ is the oxygen concentration in mg/m^3 and $\vec{j}_{O2}$ is the diffusion flux density defined by the Fick's law (2).

$$\vec{j}_{O2} = -D\frac{\partial [O_2]}{\partial t}\vec{n} \qquad (2)$$

Applying (1) to the three domains defined above, the equation can be rewritten

$$\frac{dm_{O2}}{dt} = -\oiint_{\partial DW} \vec{U}_W[O_2]\vec{n}dS - \oiint_{\partial DW} \vec{j}_{O2}\vec{n}dS - \oiint_{\partial DB} \vec{j}_{O2}\vec{n}dS \qquad (3)$$

The oxygen flux F_{O2} is only related to the bubble domain ∂D_B. Let us now consider the domain ∂D_W which is assumed to be far away from the bubble. It makes sense to assume that the perturbation induced by the bubble has disappeared, leading to ($\vec{U}_W = 0$). The last hypothesis assumes that the diffusive flux through the domain ∂D_W can be neglected compared with F_{O2}. Considerations lead to (4).

$$F_{O2} = \frac{dm_{O2}}{dt} = \lim_{\Delta t \to 0} \frac{\Delta m_{O2}}{\Delta t} = \lim_{\Delta z \to 0} \frac{\iiint [O_2] r dr d\theta dz}{\int dz / U_B} \quad (4)$$

In the spherical case, a symmetry along z axis can be considered, leading to $[O_2](r,z)$. Away from the bubble, it make also sense to assume that the variation of $[O_2]$ along z can be neglected compared with the variation along r, leading to $[O_2](r)$. Finally, the flux can be rewritten (5).

$$F_{O2} = 2\pi . U_B . \int [O_2] r dr \quad (5)$$

The flux in (5) can be easily computed since the oxygen concentration $[O_2](r)$ is proportional to a Gaussian distribution. Concerning the velocity U_B, its determination can be achieved using images recorded by the camera 2 (*cf.* Figure 2) since the delay between two successive images is known. The mass transfer coefficient in the liquid phase is then obtained by dividing the transferred flux by the bubble surface and the exchange potential in the liquid phase ($[O_2]_{saturation} - [O_2]_\infty$). Francois *et al .(*2011) have shown that the flux defined in (5) tends to a constant when the domain ∂D_W is far away enough from the bubble (about 220 bubble diameters away for a bubble with diameter of 0.72 mm). The next section present an extension to the original work presented by Francois *et al .(*2011) to the case of non-spherical bubbles.

MATHEMATICAL RESOLUTION: NON-SPHERICAL CASE

The purpose of this section is to extend the results of the spherical case to the case of non-spherical bubbles that often occur in industrial applications. The main difference in the non-spherical case is that the hypothesis of symmetry along the z axis is not longer valid for the transfer spot. Because of the diversity of the bubble shapes, depending on the bubble diameter (*cf.* Figure 4), a more general approach must be considered. The mathematical analysis of this section starts in a similar fashion to the above section until the equation (4). It is important to note that the hypothesis of absence of movement on the domain ∂D_W should be satisfied after a longer delay when compared with the spherical case. From (4) and still by assuming that the variation of $[O_2]$ according to z can be neglected compared with the variation according to r far away enough from the bubble, we obtain (6).

$$F_{O2} = \frac{dm_{O2}}{dt} = \lim_{\Delta z \to 0} \frac{\iiint [O_2] r dr d\theta dz}{\int dz / U_B} = U_B \iint [O_2] r dr d\theta \quad (6)$$

For ease for generalization, we propose to estimate the quantity $\iint [O_2] r dr d\theta$ directly from the images obtained by PLIF. More precisely, for a given image, we first estimate the noise level using a part of the image free from transfer spot. It can be seen (*cf.* Figure 6) that it is reasonable to assume that the noise (blue line in Figure 6) is Gaussian (red line in Figure 6) whose variance σ^2 can be easily estimated.

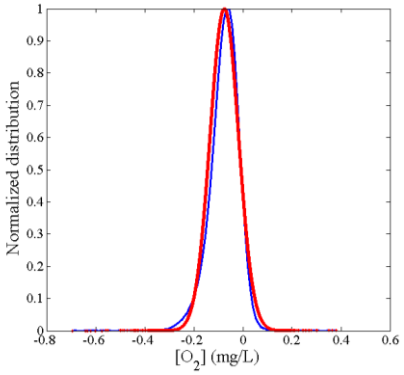

Figure 6. Fitting of the noise (blue) with a Gaussian profile (red)

The transfer spot is then estimated by keeping all pixels whose values exceed the threshold 3σ (which corresponds with a probability of about 99% that the pixels belong to the spot).

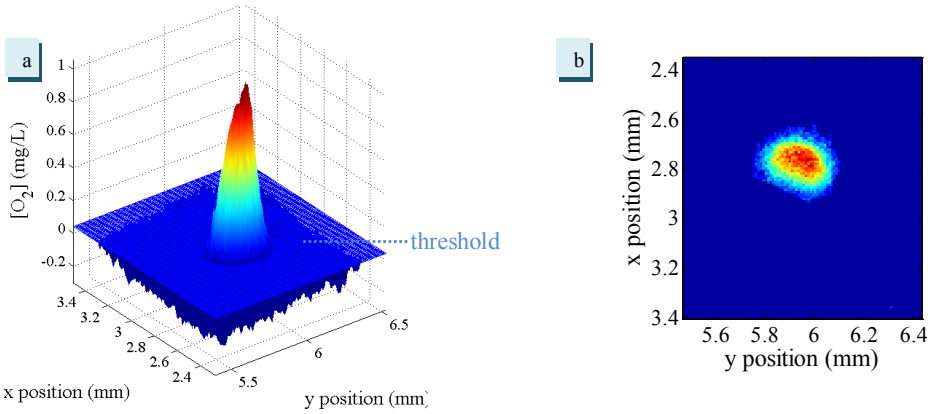

Figure 7. Visualization of mass transfer along the horizontal direction and visualization of the threshold.

Only the pixels whose values exceed the threshold are considered to estimate the integral. Figure 7-a shows the proposed threshold, where the blue plan corresponds with the threshold and the surface is the concentration profile of the transfer spot to be integrated. To estimate the integral, we propose to replace it by the discrete sum of the concentration values of interest weighted by the pixel surface as follows.

$$\iint [O_2] r dr d\theta = \sum_i [O_2]_i \delta^2 \qquad (7)$$

Where $[O_2]_i$ is the oxygen concentration of the i^{th} pixel whose value is greater than the threshold and δ is the length of any square pixel (of surface δ^2). It is important to note that the results can be deteriorated in case of too polluted media (Figure 8). The notion of "pollution" refers to the presence in oxygen in the solution due to, for instance, to previous bubbles that have transferred in the liquid phase and that altered the integral computation.

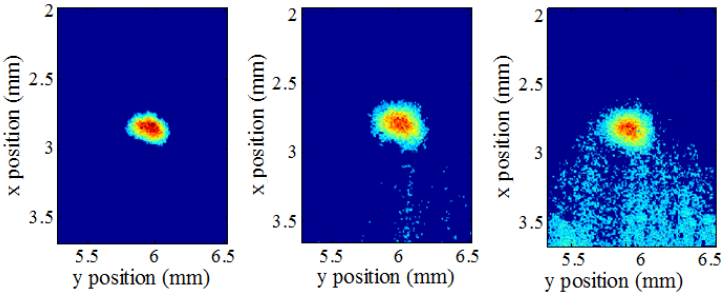

Figure 8. Evolution of the transfer spot for different times with pollution

Note that this technique for approximating $\iint [O_2] r dr d\theta$ can be applied for any shape of transfer spot, which makes the determination of the flux and the mass transfer coefficient k_L possible.

EXPERIMENTAL RESULTS

The mathematical analysis presented above has been applied for bubbles of varying diameters. For spherical bubbles, the obtained results are in good agreement with those presented in Francois *et al.* (2011). For almost spherical bubbles (of diameters up to 2 mm) (*cf.* Figure 3), the determination of the flux and thus k_L seems to be possible. The obtained values for these two parameters are intermediate values between the theoretical values of the Frössling model (fully contaminated bubbles) and the Higbie model (clean bubbles). Some experimental results obtained for that kind of bubbles in water (20°C) are shown in Table 2.

d_{bubble}	Experimental k_L (m/s)	k_L Frössling (m/s)	k_L Higbie (m/s)
1.84 mm	3×10^{-4}	1.17×10^{-4}	6.12×10^{-4}
1.94 mm	3.5×10^{-4}	1.19×10^{-4}	6.20×10^{-4}
2.1 mm	3.6×10^{-4}	1.21×10^{-4}	6.33×10^{-4}

Table2. Determination of k_L in a water/ethanol (80%m / 20%m).

The presented results correspond to a stable transfer flux (computed far away from the bubble location). In the case of bubble of diameter equals to 1.84 mm (cf. Table 2), this stabilization corresponds with a delay of about 20 images (about 400 bubble diameters) after the bubble passing to ensure that the flux has reached its asymptotic value. It is important to note that the relation proposed by Francois *et al.* (2011) for the determination of the critical distance for reaching the asymptotic state ($z_{critical}$= 20.(Reynolds)$^{0.5}$), seems to be still applicable for bubbles of larger diameters. As a consequence, the extension of the mathematical analysis and thus the studied method seems to be interesting. However, for bubbles whose diameter exceed 2.2 mm, the hydrodynamic behaviour in the wake of the bubble is more complex than in the almost spherical case and thus leads to a higher dispersion in the wake of the bubble. Recording images in the asymptotic state can be challenging. An example is depicted in Figure 9 where the mass transfer is divided into two spots and is visible only near the bubble passing (white ring).

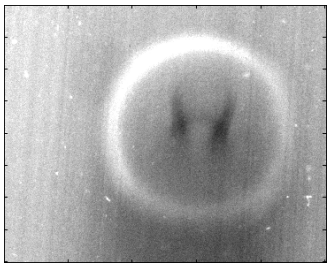

Figure 9. Complex shape of mass transfer spot ($d_{bubble}\approx$ 3mm)

To alleviate this problem, a more complex mathematical analysis should be considered for more complex hydrodynamic behaviour. One of the most important issues of the proposed method is the quality of the liquid phase that contains the bubble. More precisely, the liquid media must be perfectly free from oxygen before starting experiments in order not to disrupt the concentration profiles. Indeed, for the presented results, the measured oxygen concentration in the wake of the bubble stays under 2 mg/L, whereas the initial oxygen concentration is about 0.5 mg/L. The gap between these two values is very small, which does not allow any pollution such as pollution induced by a previously generated bubble. The related issue is to be able to generate identical bubbles one by one which is far from trivial. Despite the current limitations of the materials used in this paper, encouraging results have been obtained.

CONCLUSION

The aim of this paper was to propose an experimental set-up to visualize and locally quantify the mass transfer in the wake of a rising bubble into a liquid media. The PLIF has been used along the horizontal direction in the wake of the bubble. The studied technique has been applied to different bubble diameters. To handle the large variability of transfer spot shapes, an approximation was proposed to estimate the transferred flux and thus the liquid side mass transfer coefficient for a larger range of bubble diameters. It has been shown in this paper that the proposed technique provides accurate results for bubbles whose diameters do not exceed 2.2 mm. Another material (high speed laser) will be used to investigate the larger bubbles. Preliminary experiments using more complex media (water + salt, water + glucose …) and other gas (CO_2) are still under study and have already provided interesting results.

REFERENCES

1. Fyferling, M, 2007,Transfert d'oxygène en condition de culture microbienne intensive. PhD manuscript.

2. Geddes, CD, and JR Lakowicz, 2005, *Topics in Fluorescence Spectroscopy -Part B- Advanced concepts in fluorescence spectroscopy macromolecular sensing.* Vol. 10. Springer.

3. Stöhr, M, J Schanze, and A Khalili, 2009, Visualization of gas–liquid mass transfer and wake structure of rising bubbles using pH-sensitive PLIF. *Experiments in Fluids,* 47: 135-143.

4. Roy, S, and SR Duke, 2004, Visualization of oxygen concentration fields and measurement of concentration gradients at bubble surfaces in surfactant-contaminated water. *Experiments in Fluids,* 36: 654–662.

5. Dani, A, P Guiraud, and A Cockx, 2007, Local measurement of oxygen transfer around a single bubble by planar laser-induced fluorescence.*Chemical Engineering Science,* 62 : 7245–7252.

6. Francois, J, N Dietrich, P Guiraud, and A Cockx, 2011, Direct measurement of mass transfer around a single bubble by micro-PLIFI. *Chemical Engineering Science,* 66 : 3328-3338.

7. Stern, O, and M Volmer, 1919, On the quenching time of fluorescence.*Physik Z,* 20 : 183–188.